RodA Promotes Intestinal Colonization by Group B *Streptococcus*

Authors:

Michelle J. Vaz[a#], Sanjana Sankaran[a#], Molly E. Sharp[b], Emily Dembinski[b], Adam J. Ratner[a,b]

#Equal authorship contribution

Affiliations:

[a] Department of Pediatrics, NYU Grossman School of Medicine, New York, New York, USA

[b] Department of Microbiology, NYU Grossman School of Medicine, New York, New York, USA

*Address correspondence to Adam J. Ratner, adam.ratner@nyulangone.org

Running title: Conditional essentiality of *rodA* in GBS intestinal colonization

Key Words: *Streptococcus agalactiae (Group B Streptococcus), rodA,* gastrointestinal colonization, murine model.

Abstract:

Background. Group B *Streptococcus* (GBS) intestinal colonization is critical for the pathogenesis of late-onset (LO) disease in infants. Using a murine model, we explore the role of *rodA* which encodes a peptidoglycan polymerase RodA, belonging to the Shape, Elongation, Division, and Sporulation (SEDS) family, that participates in peptidoglycan synthesis and maintenance of cell wall integrity.

Methods. We investigated the contribution of *rodA* to GBS GI colonization, using a wild-type strain (A909 WT) and an isogenic in-frame deletion mutant of *rodA* (A909Δ*rodA*). Morphological differences between the two strains were examined by microscopy and imaging studies, and the contribution of *rodA* to GI colonization was assessed in a murine model through monocolonization and cocolonization experiments. We evaluated the growth of the mutant strain under intestinal physiological stress conditions and characterized its interactions with host epithelial cells.

Results. A909Δ*rodA* showed a unique chaining/aggregation phenotype compared to the WT strain, with the presence of capsule maintained on TEM and colony immunoblotting. In murine cocolonization experiments, A909 WT outcompeted A909Δ*rodA*; however, monocolonization experiments exhibited comparable colonization and bacterial burden across the GI tract. In vitro experiments revealed impaired growth in bile and an increase in adhesion to intestinal epithelial cells by the Δ*rodA* mutant.

Conclusion(s): *rodA* has a role in GBS intestinal colonization. Deletion of *rodA* increases sensitivity to gastrointestinal stressors in vitro and causes a pronounced defect in competition in vivo, revealing a role for cell wall polymerase in gut fitness.

45 **Introduction**

46 *Streptococcus agalactiae* (Group B *Streptococcus* [GBS]) is a leading etiology of neonatal
47 infection (1). Implementation of intrapartum antibiotic prophylaxis has markedly reduced the
48 incidence of early onset (EO) infection (occurring ≤ 7 days of life) (2, 3). However, rates of
49 maternal rectovaginal colonization persist, and the incidence of late onset (LO) infection
50 (occurring ≥7 days of life) remains unchanged, making LO disease the predominant form of
51 invasive GBS infection in infants (4, 5). Recent work has shown the incidence of LO disease
52 amongst a cohort of extremely preterm infants (< 28 weeks) as 8.47/1000 infants, nearly 30
53 times the national incidence of all neonates (6). LO disease has an overall case fatality rate of 4-
54 12%, with the rates in preterm infants being twice than that of term infants (3, 7). The sequelae
55 of LO disease include significant neurodevelopmental impairment in survivors, adding to the
56 morbidity burden (2, 8-11).

57 Prior studies have demonstrated that gastrointestinal (GI) colonization is a fundamental precursor
58 for LO infection (12, 13). Understanding how GBS establishes itself in the bacterial community
59 of the intestinal tract can uncover mechanisms that contribute to the pathogenesis of LO disease.
60 Our group recently showed the contribution of capsular polysaccharide, an important GBS
61 virulence factor, to GI fitness and colonization in a murine model of GBS intestinal colonization
62 (14). Hence, robust animal models facilitate examination of bacterial factors and host responses
63 that augment or inhibit GI colonization.

64 In this report, we explore the role of GBS *rodA*, a gene that encodes a peptidoglycan polymerase
65 called RodA, which belongs to the SEDS family proteins. RodA enables peptidoglycan
66 synthesis, which is vital for cell wall integrity, through its role as a glycosyltransferase. It is
67 known to play a role in bacterial survival under environmental stress and is relevant in bile salt

68 resistance (15, 16). Using CRISPR-Cas12a mutagenesis, we generated an in-frame deletion of
69 *rodA* in the GBS A909 background and studied its impact on cell wall structure and relation to
70 capsule, analyzed its response to intestinal physiological stressors, and determined its role in a
71 postnatal murine model of GI colonization.
72
73 **Methods**
74 All experiments were performed in accordance with the NYU Grossman School of Medicine's
75 Institutional Animal Care and Use Committee (IACUC).
76 **Bacterial Strains and Growth Conditions.** GBS WT strains A909 (serotype Ia, ST7) and its
77 derivatives were grown to stationary phase at 37°C in trypticase soy (TS) broth supplemented
78 with 5 µg/ml erythromycin as needed for selection. *Escherichia coli* strain DH5α was grown at
79 37°C, shaking in Luria-Bertani (LB) medium supplemented with 300 µg/ml erythromycin when
80 needed for selection.
81 **Construction of the GBS *rodA* deletion mutant and its complemented control strain.** The
82 *rodA* deletion mutant was created via a Cas12a-based platform as previously described
83 (17). Briefly, Cas12a-compatible GBS genomic target sites were identified by using the
84 CRISPick server hosted by the Broad Institute (18). After selecting a spacer sequence, we
85 designed custom ssDNA oligonucleotides for annealing to make a dsDNA protospacer, which
86 was then cloned into Esp3I-digested and gel-purified pGBSedit, a modified version of the
87 Cas12a-based shuttle plasmid pJC005, previously developed for *E. faecium* genetic modification
88 (19). The pGBSedit plasmid encodes an inducible Cas12a under a tightly regulated $P_{xyl/tet}$
89 promoter system responsive to anhydrotetracycline (aTC). The *rodA* gene was amplified using
90 upstream and downstream homology arms flanking the *rodA* gene using primer pairs. This

91 fragment was cloned into linearized XhoI-digested pGBSedit using Gibson assembly, followed
92 by transformation into *E. coli*. PCR followed by whole-plasmid sequencing was used to verify
93 the insert. Once cloning products had been confirmed by sequencing in *E. coli*, plasmids were
94 purified. Electrocompetent GBS was transformed with the editing plasmid and confirmed using
95 colony PCR. Colony outgrowth was performed in 10 mL TS + erythromycin 5 µg/mL culture,
96 which was allowed to grow stationary at 37 °C for 6–8 hours. These cultures were subjected to
97 anhydrotetracycline (aTC) induction, resulting in strong selection against WT strains, enabling
98 selection for homology-driven recombination mutants (20). An isolated colony was used for
99 secondary confirmation by colony PCR of genotype. Once confirmed, cultures were inoculated
100 using the genotypically confirmed colony, grown to stationary at 37°C overnight. A second
101 passage in 40 mL of TS broth was performed using 100 µL of the previous culture as inoculum.
102 1:10,000 and 1:100,000 dilutions of the grown second passage were plated on TS agar plates.
103 Colonies were dual patched onto TS and TS + 5 µg/mL Erm agar plates to detect cured clones by
104 antibiotic sensitivity profiling. All constructs were confirmed by PCR and sequencing. We
105 complemented the *rodA* gene deletion by using the pGBScomp High plasmid
106 (A909Δ*rodA*+p*rodA)* (17). Briefly, restriction digest was performed using the *SalI* restriction
107 enzyme, followed by amplification of the *rodA* gene using upstream and downstream homology
108 arms flanking the *rodA* gene and Gibson assembled with pGBScomp High. This was transformed
109 into *E.coli* followed by confirmation by sequencing. Electrocompetent GBS was transformed
110 with the editing plasmid and confirmed using colony PCR. Primers used in the construction of
111 the mutant and complemented strain are listed in **(Supplemental Table 1).** The transposon *rodA*
112 mutant (A909 *rodA::Himar1*) was used from a large-scale GBS indexed library of *Himar1* mini-
113 transposon mutant strains, containing interruptions of 878 genes and 253 intergenic regions (21).

114 **Microscopy and Staining.**

115 **Gram Stain.** WT A909 and A909Δ*rodA* strains were grown overnight in TS broth at 37 °C.
116 Cells were harvested by centrifugation (4,000 rpm, 10 min), washed once with Dulbecco's
117 phosphate-buffered saline (DPBS), and resuspended in DPBS. Smears were prepared on clean
118 glass slides, heat-fixed, and subjected to Gram staining using the standard four-step protocol:
119 crystal violet (1 min), Gram's iodine (1 min), decolorization with 95% ethanol (10–15 s), and
120 counterstaining with safranin (30 s), as previously described (22). Slides were rinsed gently with
121 distilled water between each step and air-dried. Stained preparations were examined by light
122 microscopy (1000×, oil immersion). Brightfield images were acquired using a Zeiss Axio
123 Observer microscope equipped with a 63×/1.4 oil immersion objective.

124 **Colony immunoblotting.** Overnight cultures of WT A909, A909Δ*rodA* and A909Δ*cpsE*
125 (negative control) were spread on CHROMagar plates. Colonies were counted to identify plates
126 with 20–200 colonies for subsequent immunoblotting. Plates were briefly overlaid with
127 nitrocellulose membranes (Amersham) to allow adherence of GBS material to the membrane.
128 Membranes were blocked in 3% bovine serum albumin (BSA) in DPBS (blocking solution) for 1
129 hour. Blots were then transferred to type Ia *Streptococcus* group B type antisera (Statens Serum
130 Institut) and incubated for 30 minutes with gentle shaking. Type Ia antiserum was diluted
131 1:2,000 in the blocking solution. Blots were then washed three times in DPBS. Blots were
132 incubated in horseradish peroxidase (HRP)-conjugated goat anti-rabbit secondary antibody
133 (Pierce) diluted 1:1,000 in a blocking solution for 2 hours. Blots were washed three times in
134 DPBS and stained using a 3,3′-diaminobenzidine tetrahydrochloride substrate kit (Abcam).

135 **Electron microscopy.** Overnight cultures were pelleted for 5 min at 4,000 rpm. Samples were
136 processed and imaged by the NYU Microscopy Laboratory as previously described with

137 modifications (23). In brief, bacteria were resuspended in 1 mL LRR (Lysine-Ruthenium Red-
138 Osmium) fixative solution (1 mL fixation solution per sample: 0.5 mL 0.15% ruthenium red, 125
139 µL 16% formaldehyde, 100 µL 25% glutaraldehyde solution, 0.0155 g lysine acetate; fill with
140 distilled water to 1 mL). The cells were fixed on ice for 20 min, washed two times with 0.1M
141 sodium cacodylate buffer (0.1M cacodylate, 0.01M $CaCl_2$, 0.01M $MgCl_2$, 0.09M sucrose, pH
142 6.9) containing 0.075% ruthenium red and fixed in the fixation solution without lysine acetate for
143 2 hrs on ice. After washing three times with 0.1M sodium cacodylate buffer containing 0.075%
144 ruthenium red for 5 min each, the cells were postfixed in 1% osmium tetroxide (OsO_4) with
145 0.075% ruthenium red in 0.1M sodium cacodylate buffer for 1h on ice, washed three times with
146 0.1M sodium cacodylate buffer with 0.075% ruthenium red for 5 min each, then embedded with
147 2% agar and *en block* stained with 0.5% uranyl acetate aqueous solution overnight at 4ºC. The
148 samples were washed with distilled water, dehydrated in a graded ethanol series (30%: 50%:
149 75%, 85%: 90%:100%:100%) on ice, infiltrated and embedded with LR White resin (Electron
150 Microscopy Sciences, PA) at 55ºC. Thin sections were cut using Leica UC6 ultramicrotome,
151 collected on 200 mesh copper grids (Ted, Pella Inc. CA), and stained with 4% aqueous uranyl
152 acetate for 5 minutes. Stained grids were examined under JEOL1400 Flash transmission electron
153 microscope (Japan) and photographed with a Gatan Rio 16 camera (Gatan Inc. Pleasanton, CA).
154 **GI colonization model.** These experiments were conducted as previously described (24). Two
155 cohorts were used for cocolonization: one for cocolonization with A909 WT and A909Δ*rodA*
156 strains and the other using A909 WT and A909 *rodA::Himar1*. Bacterial cultures were grown,
157 centrifuged and resuspended in sterile DPBS, and a 1:1 mixture was made of the resuspended
158 strains to be competed. Animals were orally fed using a sterile feeding tube with 10^8 CFU of
159 GBS resuspended in 50 µL of DPBS, housed with their biological dams, and monitored daily for

160 signs of illness and mortality. At predetermined time points (7- and 14-days post-infection),
161 animals were euthanized, and the GI tract was harvested. Each portion (small intestine, cecum,
162 and colon) was homogenized. Serial dilutions were plated on CHROMagar StrepB for the
163 determination of GBS colony forming units (CFUs). In addition to plating serial dilutions,
164 dilutions were spread on CHROMagar plates, with and without antibiotic selection, using glass
165 beads for the determination of strain type in A909 WT and A909 *rodA::Himar1* cohort
166 (erythromycin resistance present on transposon mutant, colonies differentiated using agar plates
167 with and without erythromycin) and by using individual colonies for colony PCR (cPCR)
168 determination in the A909 WT/A909Δ*rodA* cohort. For the monocolonization model, bacterial
169 cultures were grown overnight to stationary phase and the optical densities of the two strains
170 were normalized. Cultures were then centrifuged and resuspended in sterile DPBS to a final
171 concentration of 10^9 CFU/mL. Animals were orally fed using a sterile feeding tube with 10^8 CFU
172 of GBS resuspended in 50 µL of DPBS, respectively, and remained with their biologic, non-
173 colonized dam. The animals were monitored daily for signs of illness and mortality. At
174 predetermined time points (3-, 7-, and 14-days post-infection), animals were euthanized, and the
175 GI tract was harvested. Each portion (small intestine, cecum, and colon) was homogenized, and
176 serial dilutions were plated for determination of GBS CFUs on chromogenic agar.
177 **Colony PCR (cPCR).** Bacterial colonies were screened for the presence or absence of *rodA*
178 using cPCR. We selected ~20 random colonies per site per mouse (~100 colonies per site), which
179 was spread on CHROMagar plates. Briefly selected colonies were resuspended in 20 µL of PBS,
180 of which 2 µL was used as a template in a 25 µL PCR reaction containing OneTaq 2xMM,
181 upstream and downstream primers (Supplementary Table 1) specific for the flanking region and
182 RNAse-free water. PCR was conducted using an annealing temperature of 54°C and 2-minute

183 extension. Products were run on 1% agarose gel. Amplicon size was compared to A909 WT and
184 A909Δ*rodA* controls to confirm genotype. All colonies were counted and were classified as
185 either A909 WT or A909Δ*rodA*.
186 Competitive index for cocolonization experiments was calculated as: (CFU strain 1
187 recovered/CFU strain 1 inoculated)/(CFU strain 2 recovered/CFU strain 2 inoculated) and log-
188 transformed for calculation of geometric mean and 95% confidence interval (CI) for each GI site.
189 **Growth rate analysis under physiological stressors.** To investigate bacterial growth rate under
190 acidic pH, bile, and lysozyme conditions, overnight cultures were assayed as described
191 previously (16, 25, 26). TS broth was adjusted to pH 6.0 and 5.0 using sterile 1 N HCl. Briefly,
192 TS broth was prepared and autoclaved, cooled to room temperature (or 37 °C for temperature-
193 matched readings), and stirred aseptically while titrating with sterile 1 N HCl. pH was monitored
194 with a calibrated pH meter until 6.00 ± 0.05 and 5.00 ± 0.05 was reached. Media were re-
195 checked after 10 min equilibration, dispensed, and used the same day. Control medium (pH 7.0)
196 was handled identically without acid addition. Similarly, bile concentrations (5 mg/ml and 10
197 mg/ml) from a stock concentration of 200 mg/ml and lysozyme concentration of 14 mg/ml from
198 a stock concentration of 100 mg/ml (made in DPBS) were prepared in TSB and sterilized prior
199 use. Lysozyme concentrations were determined through preliminary testing of multiple
200 concentrations, with the final concentration selected to yield ~50% killing in the WT strain
201 (**Supplemental Figure S1)**. Overnight cultures were diluted to an OD_{600} of 0.05 in fresh TSB
202 medium, 150 µL of each culture was added to a 96-well plate in three technical replicates.
203 Media-only wells served as negative controls (blanks), and measured values were normalized by
204 subtracting the corresponding blank readings. All growth curve assays were performed using the

205 BioTek LogPhase 600 Microbiology Reader for 24 hours at 37 °C, with readings taken every 20
206 minutes.
207 **Biofilm Assay.** Biofilm assays were performed as previously described (27). Briefly, overnight
208 bacterial cultures grown in TSB were diluted to an OD_{600} of 0.05 in Todd Hewitt Broth (THB)
209 with 1% glucose, incubated for 24 hours at 37°C with 5% CO2 in 12 wells, flat bottom tissue
210 culture plates. Staining was performed the next day using 0.5% crystal violet, solubilized with
211 30% glacial acetic acid and 100uL of samples were transferred to 96 well cell culture plates for
212 readings. Spectra Max M3 was used to obtain readings at OD_{540}. Biofilms under stress conditions
213 were tested by diluting bacteria in THB 1% glucose with the relevant stress media as described
214 above.
215 **Tissue culture assays:** The human intestinal Caco-2 cell line (ATCC HTB-37; colorectal
216 adenocarcinoma) was seeded in 24-well plates at a density of 1 x 10^4 cells per well in Eagle's
217 Minimum Essential Medium (EMEM, ATCC 30-2003) supplemented with 20% (vol/vol) fetal
218 bovine serum (FBS, HyClone Cytiva, Marlborough, MA) and 1% penicillin-streptomycin
219 (Pen/Strep, 10,000 U/mL, Gibco, USA) and cultured at 37°C in a humidified 5% CO_2 incubator
220 (28). The T84 colonic epithelial cell line (ATCC CCL-248) were cultivated in Dulbecco's
221 Modified Eagle's Medium and Ham F-12 medium (DMEM: F-12, ATCC 30-2006)
222 supplemented with 10% FBS and 1% Pen/Strep (29). For adherence assays, bacterial strains
223 were grown overnight in TSB. On the day of the assay, bacterial strains were diluted to an OD_{600}
224 of 0.1, subcultured until mid-log phase. Caco-2 and T84 cells were grown to confluence in 12-
225 well and 24-well tissue culture-treated plates (Corning). One hour prior to the assay, cell culture
226 media was replaced with antibiotic - and serum-free media. Cells were washed three times with
227 DPBS prior to infection. Bacteria were washed three times with DPBS and then resuspended in

228 DMEM: F-12 or EMEM, depending on the cell type and added to cells at a multiplicity of
229 infection (MOI) of 10. Adhesion capacity was assessed after 45 minutes. Cells were washed six
230 times with DPBS, removed from plates with trypsin-EDTA, and lysed with 0.1% saponin (30).
231 Lysates were serially diluted and plated on TS agar (TSA) plates to quantify the number of
232 adherent CFU. The total number of adherent CFU was calculated as: (total CFU recovered/total
233 CFU of original inoculum) × 100%. For invasion assays, bacterial strains were prepared in the
234 same manner as for adherence. Following three washes, bacteria was added to each well, and
235 plates were incubated for 150 minutes to allow invasion. Plates were then washed six times to
236 remove non-adherent bacteria. Antibiotic-containing culture media was prepared by adding
237 gentamicin and penicillin from prepared stocks of 50 mg/mL each with a final concentration of
238 100 mg/mL gentamicin and 5 mg/mL penicillin. Plates were incubated for an additional 2 hours
239 with antibiotic media, after which invasion capacity was assessed using the same procedures
240 described for adherence. Sham experiments were performed with no bacteria and no cells to
241 serve as negative controls.
242 **Statistical Analysis.** Statistics were calculated using GraphPad Prism 10.5.0 software.
243 Colonization rates between the A909 WT and A909Δ*rodA* strains were compared using Fisher's
244 exact test. Bacterial burden comparison between the A909 WT and A909Δ*rodA* strains at
245 different GI tract sites were compared using two-way repeated measures ANOVA with Sidak's
246 multiple comparisons post-test. Biofilm formation under different stressors was evaluated using
247 two-way ANOVA with the Tukey multiple comparisons test. Tissue culture adhesion and
248 invasion assays were compared using Mann-Whitney U test.

249

250

251 **Results**

252 **Structural characterization of GBS A909Δ*rodA*:** The SEDS-family protein RodA is a
253 peptidoglycan glycosyltransferase which also acts as a polymerase, which crosslinks the glycan
254 strands, playing a key morphogenetic role in bacterial cell wall synthesis (15, 31, 32). To discern
255 the contribution of *rodA* in GI colonization, we initially employed a *rodA* transposon mutant
256 (A909 *rodA::Himar1*) as a pilot. This mutant strain was obtained through an ordered A909
257 transposon mutant library, containing over 1,900 genetic variants, each with a unique disruption
258 to its chromosome with numerous mutants (21). In cocolonization experiments, we noted that the
259 A909 WT outcompeted the A909 *rodA::Himar1,* indicating a competitive advantage in vivo
260 (**Supplemental Figure S2).** To explore the mechanism of these findings, we generated an in-
261 frame deletion mutant (A909Δ*rodA)* using the Cas12a mutagenesis system as previously
262 described (17). Overnight growth showed pronounced sedimentation of the A909Δ*rodA*
263 compared to the A909 WT strain and complemented A909Δ*rodA*+p*rodA*, although no
264 significant differences were noted with no alteration in long term (24 hours) growth assays
265 **(Supplemental Figure S3, Figure 4A)**. Gram staining revealed a typical streptococcal
266 morphology, with chains of cocci in the WT strain. We noted a marked aggregation phenotype,
267 with cells forming dense clusters versus discrete chains, in the A909Δ*rodA* strain **(Figure 1A).**
268 We assessed capsule production to determine if *rodA* played a role in its production. Colony
269 immunoblotting detected capsule formation by both the A909 WT and A909 Δ*rodA* strains in
270 contrast to the A909Δ*cpsE,* which did produce detectable capsule (**Figure 1B).** In addition, we
271 confirmed the presence of capsule production in the A909Δ*rodA* strain by latex agglutination
272 (**Figure 1C).** Transmission electron microscopy revealed no discernible differences in cell shape,
273 size, or cell envelope in the A909Δ*rodA* strain compared to the A909 WT strain **(Figure 1D)**.

274 These findings suggest a phenotype with chaining and aggregation in the A909Δ*rodA* strain,
275 without an overt structural or capsule deficit.

276 ***rodA* provides a competitive advantage in GI colonization.** To assess the contribution of *rodA*
277 to intestinal colonization, we examined the A909Δ*rodA* strain in a murine model. Preweaning
278 mice (12–14 days) were orally infected in cocolonization experiments as described (24). Animals
279 cocolonized with the A909 WT and A909Δ*rodA* strains were monitored for signs of illness and
280 survival until 7 days post infection. There was 100% survival in this cohort at the experimental
281 endpoint of 7 days, at which point animals were euthanized and the GI tract harvested **(Figure**
282 **2A)**. Colonies were analyzed using cPCR to amplify for WT or KO bands **(Supplemental**
283 **Figure 4)**. In the small intestine and cecum, the A909 WT strain outcompeted the A909Δ*rodA*
284 strain with a geometric mean competitive index of 40, 95% CI [40, 40] at 7 days post-
285 colonization, denoting no variation across replicates, as all tested colonies were A909 WT
286 **(Figure 2B)**. In the colon, we calculated a geometric mean of 34.47, 95% CI [22.8, 52.11]
287 **(Figure 2B)**. These data are consistent with the findings noted in cocolonization experiments
288 using the transposon mutant A909 *rodA::Himar1* and A909 WT which showed geometric mean
289 competitive indices 6.62, 95% CI [0.85, 53.1] and 4.19, 95% CI [1.70, 10.35] in the small
290 intestine; 7.67, 95% CI [1.69, 34.8] and 45.78, 95% CI [10.38, 201.7] in the cecum, and 7.5, 95%
291 CI [1.68, 33.76] and 49.82, 95% CI [17.72, 140.1] in the colon, at 7 and 14 days respectively
292 **(Supplemental Figure S2)**. These findings suggest a sustained competitive advantage of the
293 A909 WT strain over the A909Δ*rodA* strain throughout the GI tract.

294 ***rodA* is dispensable for intestinal colonization in the absence of competition.** We next
295 performed monocolonization experiments to determine the mechanism of the colonization
296 advantage. In longitudinal experiments across multiple cohorts, pre-weaning mice were orally

297 infected with either the A909 WT strain or the A909Δ*rodA* strain. These animals were
298 longitudinally monitored for signs or illness/mortality, with cohorts euthanized at days 3, 7 or 14.
299 We noted equivalent bacterial colonization between the WT and KO strain throughout the GI
300 tract at all 3 time points **(Figure 3 A, C, E)**. On further assessment, we noted comparable
301 recovery of bacterial burden throughout the GI tract, except in the colon at day 3 and day 7 post
302 colonization, where the A909 WT strain had a higher median colonization density than the KO
303 strain **(Figure 3 B, D, F)**. There was an overall decrease in bacterial burden at day 14 post
304 infection, across strains **(Figure 3F)**. Taken together, we note that the A909Δ*rodA* demonstrated
305 adequate colonization efficacy in monocolonization experiments; however, it was outcompeted
306 by the WT GBS strain in cocolonization. This suggests that *rodA* may not be strictly essential for
307 establishment of intestinal colonization but may confer a selective advantage under competitive
308 pressure.

309 **Investigating *rodA* response to intestinal physiological stress:** To further characterize the role
310 of *rodA* in the GI tract, we explored bacterial growth in vitro in the presence of physiological
311 gastrointestinal stress conditions. We monitored growth of A909 WT, A909Δ*rodA* and
312 complemented strain (A909Δ*rodA*+p*rodA*) in TSB medium with acidic pH in the range of 5.0-
313 7.34, bile concentrations of 5 mg/mL, 10 mg/mL and lysozyme (14 mg/ml). The growth of all
314 three strains were unaffected by a pH of 6, however there was an overall decrease in growth rate
315 and bacterial mass at a pH of 5 in both groups **(Figure 4B, C)**. The growth of A909Δ*rodA* was
316 inhibited in both bile salt concentrations, with the WT strain growing in both conditions and the
317 complemented strain exhibiting partial restoration of growth at both bile concentrations **(Figure**
318 **4D, E)**. We noted no significant difference in growth in both strains in the presence of lysozyme
319 **(Figure 4F)**. In all assays, the complemented strain showed a delay in entry into log phase, likely

320 due to growth antibiotic selection pressure. Together these findings suggest that *rodA* is not
321 required for survival under acid stress and does not contribute to lysozyme resistance, but it is
322 required for optimal growth in the presence of bile salts.

323 ***rodA* influences bacterial surface contact and host interactions**: As biofilm formation and
324 adhesion to host epithelial surfaces are both important for gastrointestinal persistence, we next
325 examined whether deletion of *rodA* altered these phenotypes. We assessed the formation of
326 biofilm in A909 WT and A909Δ*rodA* strains after exposure to acidic media, lysozyme and bile.
327 At pH 6.0, no difference was noted in biofilm production between the WT and KO strains
328 **(Figure 5A)**. At pH 5.0, the A909Δ*rodA* strain exhibited a decrease in biofilm production
329 compared to its control (standard media, pH 7.34) **(Figure 5B)**. On exposure to lysozyme, we
330 noted an increase in biofilm formation by the A909 WT strain that was not seen in the
331 A909Δ*rodA* strain **(Figure 5C)**. The presence of bile salts impacted the formation of biofilm in
332 both the WT and KO strains equally when compared to their respective controls **(Figure 5D, E)**.
333 To understand the surface associated behavior of *rodA* at epithelial barriers, we performed
334 adherence and invasion assays using differentiated Caco-2 intestinal epithelial cells and T84
335 colonic epithelial cell lines, in an in vitro model. We evaluated if the adherence and/or invasion
336 to epithelial cells by GBS depended on the presence of *rodA*. Adherence assays showed an
337 increased adherence by the A909Δ*rodA* strain in the Caco-2 and T84 cell lines compared to the
338 A909 WT strain **(Figure 6A, B)**. In contrast, invasion assay results differed by cell type. In
339 Caco-2 cell, there was no difference in invasion between the WT and KO strains, whereas in T84
340 cells, there was an increase in invasion by the A909Δ*rodA* strain **(Figure 6C, D)**. These findings
341 suggest that *rodA* influences bacterial and host interactions in a contextual manner, rather than a
342 uniform effect.

343 **Discussion**

344 The GBS cell wall has a thick gram positive layer composed of peptidoglycan, which anchors
345 surface molecules like the group B carbohydrate) and an outermost boundary of capsular
346 polysaccharide that serves as a major factor in colonization and pathogenesis (33),(34, 35),(36).
347 SEDS proteins are essential transmembrane enzymes and have emerged as essential meditators
348 of peptidoglycan synthesis and cell wall integrity (37). The role of the peptidoglycan layer and
349 bacterial pathogenesis have been explored in other enteric pathogens (38, 39). Laubacher et al.
350 demonstrated that peptidoglycan damage led to an increase in capsule synthesis, allowing for *E.*
351 *coli* survival in the presence of antibiotics.(39) RodA, a member of the SEDS family, is a
352 peptidoglycan polymerase contributing to bacterial shape and cell wall integrity (40). Prior
353 reports have shown that the deletion of *rodA* leads to a loss of structure as seen in *Streptococcus*
354 *pneumoniae*, *E. coli*, *Salmonella* and *Bacillus subtilis* (41-44). Deletion of the either *rodA* or
355 genes encoding penicillin-binding proteins (PBPs), which play a key role in peptidoglycan
356 synthesis, has been shown to cause a downregulation of cell invasion-associated virulence
357 factors like flagella, in vitro and in vivo, in *Salmonella* (45). In *M. tuberculosis*, the absence of
358 RodA and PbpA did not impact growth in vitro, however, both were found to be required for
359 bacterial survival in a guinea pig infection model (46). Prior reports have shown that in GBS,
360 RodA works in conjunction with a PBP complex during the process of peptidoglycan synthesis
361 (47). In keeping with our findings, Jia et al. reported the conditional essentiality of *rodA* gene to
362 bile salt resistance by GBS (16). In this report, we characterized the role of *rodA* in GBS and
363 examined its contribution to membrane stability, response to intestinal stressors in vitro, and
364 intestinal colonization in a murine model.

365 In a model of GI colonization, we noted that the A909Δ*rodA* mutant displayed adequate
366 colonization during monocolonization but was significantly outcompeted by the WT strain
367 during cocolonization. This suggests that *rodA* is not essential for intestinal colonization but may
368 confer an advantage under competitive pressure. This phenomenon of competitive interactions
369 has been described in other enteric pathogens and is likely dependent on host, microbial, or
370 nutritional pressures that become apparent during competition (48-50). We noted comparable
371 bacterial burden across different sites of the GI tract, except the colon, in longitudinal
372 experiments.

373 Exposure to intestinal physiological stressors like acid, bile and lysozyme showed that *rodA* is
374 important for bile tolerance and biofilm adaptation to certain stressors. We hypothesize that
375 absence of *rodA* may decrease the number of cross-links between glycan chains making the cell
376 membrane more permeable, explaining the bile susceptibility which disrupts the bacterial cell
377 wall by causing cell membrane leakage and denature proteins. Also, deletion of *rodA* may alter
378 the PBP complex or prevent the activation of envelope stress pathways as seen in *B. subtilis*,
379 making the A909Δ*rodA* vulnerable to the above stressors. Thibessard et al. have also
380 demonstrated that the lack of RodA or PBP2b leads to loss of oxidative stress resistance in
381 *Streptococcus thermophilus* (51). Structural characterization revealed a chaining/aggregating
382 effect by A909Δ*rodA* on gram staining, but we did not detect changes to the bacterial shape as
383 previously noted in *Streptococcus pneumoniae* or cell division as noted with *Streptococcus*
384 *thermophilus* (44, 51). We propose that the aggregating phenomenon likely reflects impaired cell
385 separation due to subtle changes in peptidoglycan remodeling or surface charge, rather than a
386 direct defect in division or capsule synthesis. This dual effect may contribute to the increased
387 adherence by the A909Δ*rodA* strain in in vitro epithelial cell lines with cell type specific

388 responses to invasion - higher in the T84 than the Caco-2 cell line. These differences may reflect
389 specific characteristics of the host epithelial surface, including mucus production or barrier
390 integrity – suggesting that the effect of *rodA* on host interactions are more dynamic in the gut.

391 The context-dependent role of RodA uncovered in this report reflects its biological relevance
392 under stress/competition. It also highlights the importance of RodA as a potential target for
393 antibiotic therapy. It gives us a window into the dynamic microbial changes that occur in a
394 natural setting during colonization persistence and/or clearance. Applying genomic sequencing
395 methods may help us identify and understand many other conditional essential genes like *rodA*
396 that confer a competitive advantage and inform strategies to disrupt colonization and
397 transmission in the GI tract.

398 **ACKNOWLEDGMENTS**

399 **Funding.** This work was supported by grant R01AI155476 to A.J.R. The content is solely the
400 responsibility of the authors and does not necessarily represent the official views of the funding
401 bodies. We thank NYULH Microscopy Lab (partially supported by NYU Cancer Center Support
402 Grant NIH/NCI P30CA016087) for consultation and preparation of the electron microscopy
403 images.

404 **Potential conflicts of interest.** The authors declare that they have no conflicts of interest.

405 **Author Notes.** This work was presented in part at the Pediatric Academic Societies' 2025
406 Annual Meeting.

407

408

409 **References**

410 1. Malvolti S, Pecenka C, Mantel CF, Malhame M, Lambach P. 2022. A Financial and
411 Global Demand Analysis to Inform Decisions for Funding and Clinical Development of
412 Group B *Streptococcus* Vaccines for Pregnant Women. Clin Infect Dis 74:S70-S79.
413 2. Puopolo KM, Lynfield R, Cummings JJ, Committee On Fetus And Newborn; Committee
414 On Infectious Diseases. 2019. Management of Infants at Risk for Group B Streptococcal
415 Disease. Pediatrics 144: e20191881.
416 3. Nanduri SA, Petit S, Smelser C, Apostol M, Alden NB, Harrison LH, Lynfield R,
417 Vagnone PS, Burzlaff K, Spina NL, Dufort EM, Schaffner W, Thomas AR, Farley MM,
418 Jain JH, Pondo T, McGee L, Beall BW, Schrag SJ. 2019. Epidemiology of Invasive
419 Early-Onset and Late-Onset Group B Streptococcal Disease in the United States, 2006 to
420 2015: Multistate Laboratory and Population-Based Surveillance. JAMA Pediatr 173:224-
421 233.
422 4. Centers for Disease Control and Prevention. 2023. Active bacterial core surveillance
423 report, emerging infections program network, Group B *Streptococcus*, 2023.
424 https://www.cdc.gov/abcs/downloads/GBS_Surveillance_Report_2023.pdf. Accessed 20
425 September 2025.
426 5. Karampatsas K, Davies H, Mynarek M, Andrews N, Heath PT, Le Doare K. 2022.
427 Clinical Risk Factors Associated With Late-Onset Invasive Group B Streptococcal
428 Disease: Systematic Review and Meta-Analyses. Clin Infect Dis 75:1255-1264.
429 6. Puopolo KM, Mukhopadhyay S, Hansen NI, Flannery DD, Greenberg RG, Sanchez PJ,
430 Bell EF, DeMauro SB, Wyckoff MH, Eichenwald EC, Stoll BJ. 2022. Group B
431 *Streptococcus* Infection in Extremely Preterm Neonates and Neurodevelopmental
432 Outcomes at 2 Years. Clin Infect Dis 75:1405-1415.
433 7. Madrid L, Seale AC, Kohli-Lynch M, Edmond KM, Lawn JE, Heath PT, Madhi SA,
434 Baker CJ, Bartlett L, Cutland C, Gravett MG, Ip M, Le Doare K, Rubens CE, Saha SK,
435 Sobanjo-Ter Meulen A, Vekemans J, Schrag S, Infant GBS Disease Investigator Group.
436 2017. Infant Group B Streptococcal Disease Incidence and Serotypes Worldwide:
437 Systematic Review and Meta-analyses. Clin Infect Dis 65:S160-S172.
438 8. Berardi A, Lugli L, Rossi C, China MC, Vellani G, Contiero R, Calanca F, Camerlo F,
439 Casula F, Di Carlo C, Rossi MR, Chiarabini R, Ferrari M, Minniti S, Venturelli C,
440 Silvestrini D, Dodi I, Zucchini A, Ferrari F, Infezioni da Streptococco B Della Regione
441 Emilia Romagna. 2010. Neonatal bacterial meningitis. Minerva Pediatr 62:51-54.
442 9. Libster R, Edwards KM, Levent F, Edwards MS, Rench MA, Castagnini LA, Cooper T,
443 Sparks RC, Baker CJ, Shah PE. 2012. Long-term outcomes of group B streptococcal
444 meningitis. Pediatrics 130:e8-15.
445 10. Kohli-Lynch M, Russell NJ, Seale AC, Dangor Z, Tann CJ, Baker CJ, Bartlett L, Cutland
446 C, Gravett MG, Heath PT, Ip M, Le Doare K, Madhi SA, Rubens CE, Saha SK, Schrag S,
447 Sobanjo-Ter Meulen A, Vekemans J, O'Sullivan C, Nakwa F, Ben Hamouda H, Soua H,
448 Giorgakoudi K, Ladhani S, Lamagni T, Rattue H, Trotter C, Lawn JE. 2017.
449 Neurodevelopmental Impairment in Children After Group B Streptococcal Disease
450 Worldwide: Systematic Review and Meta-analyses. Clin Infect Dis 65:S190-S199.
451 11. Goncalves BP, Procter SR, Paul P, Chandna J, Lewin A, Seedat F, Koukounari A,
452 Dangor Z, Leahy S, Santhanam S, John HB, Bramugy J, Bardaji A, Abubakar A,
453 Nasambu C, Libster R, Sanchez Yanotti C, Horvath-Puho E, Sorensen HT, van de Beek

454 D, Bijlsma MW, Gardner WM, Kassebaum N, Trotter C, Bassat Q, Madhi SA, Lambach
455 P, Jit M, Lawn JE, GBS Danish and Dutch collaborative group for long term outcomes;
456 GBS Low and Middle Income Countries collaborative group for long term outcomes;
457 GBS Scientific Advisory Group, epidemiological sub-group; CHAMPS team. 2022.
458 Group B *Streptococcus* infection during pregnancy and infancy: estimates of regional and
459 global burden. Lancet Glob Health 10:e807-e819.
460 12. Carl MA, Ndao IM, Springman AC, Manning SD, Johnson JR, Johnston BD, Burnham
461 CA, Weinstock ES, Weinstock GM, Wylie TN, Mitreva M, Abubucker S, Zhou Y,
462 Stevens HJ, Hall-Moore C, Julian S, Shaikh N, Warner BB, Tarr PI. 2014. Sepsis from
463 the gut: the enteric habitat of bacteria that cause late-onset neonatal bloodstream
464 infections. Clin Infect Dis 58:1211-1218.
465 13. Schwartz DJ, Shalon N, Wardenburg K, DeVeaux A, Wallace MA, Hall-Moore C, Ndao
466 IM, Sullivan JE, Radmacher P, Escobedo M, Burnham CD, Warner BB, Tarr PI, Dantas
467 G. 2023. Gut pathogen colonization precedes bloodstream infection in the neonatal
468 intensive care unit. Sci Transl Med 15:eadg5562.
469 14. Vaz MJ, Purrier SA, Bonakdar M, Chamby AB, Ratner AJ, Randis TM. 2020. The
470 Impact of Circulating Antibody on Group B *Streptococcus* Intestinal Colonization and
471 Invasive Disease. Infect Immun 89:e00348-20.
472 15. Welsh MA, Schaefer K, Taguchi A, Kahne D, Walker S. 2019. Direction of Chain
473 Growth and Substrate Preferences of Shape, Elongation, Division, and Sporulation-
474 Family Peptidoglycan Glycosyltransferases. J Am Chem Soc 141:12994-12997.
475 16. Jia L, Yuan C, Pan F, Zhou X, Fan H, Ma Z. 2023. CsbD, a Novel Group B Streptococcal
476 Stress Response Factor That Contributes to Bacterial Resistance against Environmental
477 Bile Salts. J Bacteriol 205:e0044822.
478 17. Hillebrand GH, Carlin SC, Giacobe EJ, Stephenson HA, Collins J, Hooven TA. 2025. A
479 Cas12a Toolbox for Rapid and Flexible Group B *Streptococcus* Genomic Editing and
480 CRISPRi. Mol Microbiol doi:10.1111/mmi.70022.
481 18. Nunez Pedrozo CN, Peralta TM, Olea FD, Locatelli P, Crottogini AJ, Belaich MN,
482 Cuniberti LA. 2022. In silico performance analysis of web tools for CRISPRa sgRNA
483 design in human genes. Comput Struct Biotechnol J 20:3779-3782.
484 19. Chua MJ, Collins J. 2022. Rapid, Efficient, and Cost-Effective Gene Editing of
485 *Enterococcus faecium* with CRISPR-Cas12a. Microbiol Spectr 10:e0242721.
486 20. Helle L, Kull M, Mayer S, Marincola G, Zelder ME, Goerke C, Wolz C, Bertram R.
487 2011. Vectors for improved Tet repressor-dependent gradual gene induction or silencing
488 in *Staphylococcus aureus*. Microbiology (Reading) 157:3314-3323.
489 21. Bhavana VH, Hillebrand GH, Gopalakrishna KP, Rapp RA, Ratner AJ, Tettelin H,
490 Hooven TA. 2023. A Group B *Streptococcus* indexed transposon mutant library to
491 accelerate genetic research on an important perinatal pathogen. Microbiol Spectr
492 11:e0204623.
493 22. Moyes RB, Reynolds J, Breakwell DP. 2009. Differential staining of bacteria: gram stain.
494 Curr Protoc Microbiol Appendix 3:Appendix 3C.
495 23. Hammerschmidt S, Wolff S, Hocke A, Rosseau S, Muller E, Rohde M. 2005. Illustration
496 of pneumococcal polysaccharide capsule during adherence and invasion of epithelial
497 cells. Infect Immun 73:4653-4667.
498 24. Vaz MJ, Dongas S, Ratner AJ. 2023. Capsule production promotes Group B
499 *Streptococcus* intestinal colonization. Microbiol Spectr 11:e0234923.

500 25. Yang Q, Porter AJ, Zhang M, Harrington DJ, Black GW, Sutcliffe IC. 2012. The impact
501 of pH and nutrient stress on the growth and survival of *Streptococcus agalactiae*. Antonie
502 Van Leeuwenhoek 102:277-287.
503 26. Patras KA, Derieux J, Al-Bassam MM, Adiletta N, Vrbanac A, Lapek JD, Zengler K,
504 Gonzalez DJ, Nizet V. 2018. Group B *Streptococcus* Biofilm Regulatory Protein A
505 Contributes to Bacterial Physiology and Innate Immune Resistance. J Infect Dis
506 218:1641-1652.
507 27. D'Urzo N, Martinelli M, Pezzicoli A, De Cesare V, Pinto V, Margarit I, Telford JL,
508 Maione D, Members of the DEVANI Study Group. 2014. Acidic pH strongly enhances in
509 vitro biofilm formation by a subset of hypervirulent ST-17 *Streptococcus agalactiae*
510 strains. Appl Environ Microbiol 80:2176-2185.
511 28. De Gaetano GV, Lentini G, Galbo R, Coppolino F, Fama A, Teti G, Beninati C. 2021.
512 Invasion and trafficking of hypervirulent group B streptococci in polarized enterocytes.
513 PLoS One 16:e0253242.
514 29. Dominguez K, Pearah AN, Lindon AK, Worthington LA, Carter RR, John-Lewis
515 Edwards N, Ho TTB, Darch SE, Randis TM. 2024. The impact of butyrate on group B
516 *Streptococcus*-induced intestinal barrier disruption. Infect Immun 92:e0020024.
517 30. Yang Q, Li N, Zheng Y, Tian Y, Liang Q, Zhao M, Chu H, Gong Y, Wu T, Wei S, Wang
518 H, Yan G, Li F, Lei L. 2025. Identification and characterization of *ugpE* associated with
519 the full virulence of *Streptococcus suis*. Vet Res 56:82.
520 31. Emami K, Guyet A, Kawai Y, Devi J, Wu LJ, Allenby N, Daniel RA, Errington J. 2017.
521 RodA as the missing glycosyltransferase in *Bacillus subtilis* and antibiotic discovery for
522 the peptidoglycan polymerase pathway. Nat Microbiol 2:16253.
523 32. Cho H, Wivagg CN, Kapoor M, Barry Z, Rohs PDA, Suh H, Marto JA, Garner EC,
524 Bernhardt TG. 2016. Bacterial cell wall biogenesis is mediated by SEDS and PBP
525 polymerase families functioning semi-autonomously. Nat Microbiol 1:16172.
526 33. Silhavy TJ, Kahne D, Walker S. 2010. The bacterial cell envelope. Cold Spring Harb
527 Perspect Biol 2:a000414.
528 34. Wessels MR, Rubens CE, Benedi VJ, Kasper DL. 1989. Definition of a bacterial
529 virulence factor: sialylation of the group B streptococcal capsule. Proc Natl Acad Sci U S
530 A 86:8983-8987.
531 35. Rosini R, Margarit I. 2015. Biofilm formation by *Streptococcus agalactiae*: influence of
532 environmental conditions and implicated virulence factors. Front Cell Infect Microbiol
533 5:6.
534 36. Kampff Z, van Sinderen D, Mahony J. 2023. Cell wall polysaccharides of streptococci: A
535 genetic and structural perspective. Biotechnol Adv 69:108279.
536 37. Meeske AJ, Riley EP, Robins WP, Uehara T, Mekalanos JJ, Kahne D, Walker S, Kruse
537 AC, Bernhardt TG, Rudner DZ. 2016. SEDS proteins are a widespread family of
538 bacterial cell wall polymerases. Nature 537:634-638.
539 38. Ranjit DK, Young KD. 2013. The Rcs stress response and accessory envelope proteins
540 are required for de novo generation of cell shape in *Escherichia coli*. J Bacteriol
541 195:2452-2462.
542 39. Laubacher ME, Ades SE. 2008. The Rcs phosphorelay is a cell envelope stress response
543 activated by peptidoglycan stress and contributes to intrinsic antibiotic resistance. J
544 Bacteriol 190:2065-2074.

545 40. Emami K, Guyet A, Kawai Y, Devi J, Wu LJ, Allenby N, Daniel RA, Errington J. 2017.
546 Corrigendum: RodA as the missing glycosyltransferase in *Bacillus subtilis* and antibiotic
547 discovery for the peptidoglycan polymerase pathway. Nat Microbiol 2:17019.
548 41. Bendezu FO, Hale CA, Bernhardt TG, de Boer PA. 2009. *RodZ* (*YfgA*) is required for
549 proper assembly of the MreB actin cytoskeleton and cell shape in *E. coli*. EMBO J
550 28:193-204.
551 42. Wei Y, Havasy T, McPherson DC, Popham DL. 2003. Rod shape determination by the
552 *Bacillus subtilis* class B penicillin-binding proteins encoded by *pbpA* and *pbpH*. J
553 Bacteriol 185:4717-4726.
554 43. Henriques AO, Glaser P, Piggot PJ, Moran CP, Jr. 1998. Control of cell shape and
555 elongation by the *rodA* gene in *Bacillus subtilis*. Mol Microbiol 28:235-247.
556 44. Lamanna MM, Manzoor I, Joseph M, Ye ZA, Benedet M, Zanardi A, Ren Z, Wang X,
557 Massidda O, Tsui HT, Winkler ME. 2022. Roles of *RodZ* and class A PBP1b in the
558 assembly and regulation of the peripheral peptidoglycan elongasome in ovoid-shaped
559 cells of *Streptococcus pneumoniae* D39. Mol Microbiol 118:336-368.
560 45. Doble AC, Clark-Corrigall J, Bulmer DM, Daniel RA, Mastroeni P, Anjam Khan CM.
561 2024. Essential roles of RodA peptidoglycan polymerase and PBP2 transpeptidase in
562 expression of cell wall-spanning supramolecular organelles and
563 modulating *Salmonella* virulence. bioRxiv [Preprint]. doi:10.1101/2024.07.01.601524.
564 46. Arora D, Chawla Y, Malakar B, Singh A, Nandicoori VK. 2018. The transpeptidase
565 PbpA and noncanonical transglycosylase RodA of *Mycobacterium tuberculosis* play
566 important roles in regulating bacterial cell lengths. J Biol Chem 293:6497-6516.
567 47. Zhu L, Yerramilli P, Pruitt L, Mishra A, Olsen RJ, Beres SB, Waller AS, Musser JM.
568 2021. Functional Insights into the High-Molecular-Mass Penicillin-Binding Proteins of
569 *Streptococcus agalactiae* Revealed by Gene Deletion and Transposon Mutagenesis
570 Analysis. J Bacteriol 203:e0023421.
571 48. Li SH, Li Z, Park JO, King CG, Rabinowitz JD, Wingreen NS, Gitai Z. 2018.
572 *Escherichia coli* translation strategies differ across carbon, nitrogen and phosphorus
573 limitation conditions. Nat Microbiol 3:939-947.
574 49. Liu H, Shiver AL, Price MN, Carlson HK, Trotter VV, Chen Y, Escalante V, Ray J, Hern
575 KE, Petzold CJ, Turnbaugh PJ, Huang KC, Arkin AP, Deutschbauer AM. 2021.
576 Functional genetics of human gut commensal *Bacteroides thetaiotaomicron* reveals
577 metabolic requirements for growth across environments. Cell Rep 34:108789.
578 50. Stubbendieck RM, May DS, Chevrette MG, Temkin MI, Wendt-Pienkowski E, Cagnazzo
579 J, Carlson CM, Gern JE, Currie CR. 2019. Competition among Nasal Bacteria Suggests a
580 Role for Siderophore-Mediated Interactions in Shaping the Human Nasal Microbiota.
581 Appl Environ Microbiol 85:e00637-19.
582 51. Thibessard A, Fernandez A, Gintz B, Leblond-Bourget N, Decaris B. 2002. Effects of
583 *rodA* and pbp2b disruption on cell morphology and oxidative stress response of
584 *Streptococcus thermophilus* CNRZ368. J Bacteriol 184:2821-2826.
585

586

587

588 **Figure Legends**

589 **Figure 1. Structural characterization of WT and *rodA* deficient GBS. A**. Gram-stained
590 images of A909 WT and A909Δ*rodA* strains in stationary growth, taken at 63×original
591 magnification. Scale bar = 5 µm. Experiments were performed twice independently, with
592 representative images shown. **B.** Capsule production assessed by colony immunoblot using a
593 serotype Ia-specific anti-capsular polysaccharide antibody in A909 WT, A909Δ*cpsE* (control)
594 and A909Δ*rodA* strains. Positive: Halo around brown colonies; Negative: brown colonies only.
595 Representative blot from two independent experiments is shown. **C.** Latex agglutination was
596 used to confirm production of capsule. Type Ia antisera was used for A909 WT, A909 Δ*cpsE*
597 (control) and A909Δ*rodA* strains. Positive: clumping noted; Negative: no clumping noted.
598 Representative blot from two independent experiments is shown. **D.** Transmission electron
599 microscopy demonstrate capsule and cell wall in A909 WT and A909Δ*rodA* strains. Bacteria
600 were chemically fixed by including lysine acetate during the glutaraldehyde and formaldehyde
601 exposure. Samples were stained and postfixed using Ruthenium red and osmium and
602 subsequently embedded in LR White. Black arrows mark the capsule, and white arrows mark the
603 cell wall. Scale bar = 200 nm.

604 **Figure 2. RodA confers a competitive advantage to GBS in an intestinal colonization**
605 **competition model.** Preweaning C57BL/6J mice were orally inoculated with a 1:1 mixture of
606 A909 WT and A909Δ*rodA* in an experimental cohort (n = 5). **A.** Kaplan-Meier survival curve
607 demonstrates 100% survival. **B.** The small intestine, cecum, and colon, were harvested at 7 days
608 post inoculation. Approximately 100 colonies per GI site (~20 colonies per mouse) were
609 analyzed using colony PCR to differentiate between A909 WT and A909Δ*rodA*. Data points
610 represent geometric mean competition indices and error bars represent 95% confidence intervals.

611 **Figure 3. Comparable colonization by the A909Δ*rodA* mutant and A909 WT strains in**
612 **monocolonization.** Preweaning C57BL/6J mice were orally infected with either A909 WT or
613 A909Δ*rodA* in six separate cohorts, and the small intestine, cecum, and colon, were harvested at
614 predetermined time intervals. **A, B, C.** Percent colonization as determined by the presence of
615 GBS on days 3, 7 and 14 respectively (P = not significant [NS]; two-sided Fisher's exact test). **D,**
616 **E, F.** Bacterial burden determined as GBS CFU/gram tissue on days 3,7 and 14 respectively.
617 Individual points represent biologic replicates and lines showing median with interquartile range,
618 (*, $p<0.01$; **, $p<0.001$; two-way repeated measures ANOVA with Sidak's multiple
619 comparisons post-test). Sample sizes: n=A909 WT=4, A909Δ*rodA*=7 **(Figure A, D)**, n=A909
620 WT = 5, A909Δ*rodA* = 7 **(Figure B, E)**, n=A909 WT=4, A909Δ*rodA* = 6 **(Figure C, F)**.

621 **Figure 4. Exposure to intestinal physiological stressors reveals selective susceptibility of**
622 **A909Δ*rodA*.** Overnight cultures of A909 WT, A909Δ*rodA* and A909Δ*rodA*+p*rodA* GBS strains
623 were diluted to an OD value of 0.05 in Todd-Hewitt broth and incubated at 37°C. OD_{600} was
624 measured at 20-miNute intervals under different intestinal stressors. **A.** Standard media (pH
625 7.34), **B.** Standard media, pH 6.0, **C.** Standard media, pH 5.0, **D.** Standard media, bile 5 mg/ml
626 (0.5%), **E**. Standard media, bile 10 mg/ml (1.0%), **F.** Standard media, lysozyme 14 mg/ml. Data
627 from independent samples (n = 9) with three technical replicates shown, with lines indicating
628 mean values ± standard errors of the mean (SEM).

629 **Figure 5. GBS *rodA* deficiency impacts biofilm formation under select stressor exposure.**
630 Biofilm formation of A909 WT and A909Δ*rodA* strains quantified by crystal violet uptake after
631 exposure to **A.** THB, with 1% glucose at pH 6.0, **B.** THB, with 1% glucose at pH 5.0, **C.** THB,
632 with 1% glucose, lysozyme 14 mg/ml, **D.** THB, with 1% glucose, bile 5 mg/ml, **E.** THB, with
633 1% glucose, bile 10 mg/ml. Data from independent samples (n = 9) with three technical

634 replicates are shown, and lines represent mean values ± SDs. Data were analyzed using two-way
635 ANOVA with the Tukey multiple comparisons test (*, $p<0.05$; **, $p<0.005$; ****$p< 0.0001$).

636 **Figure 6. The absence of *rodA* impacts adherence but not invasion in intestinal epithelial**
637 **cells. A, C.** Adhesion assays were performed with Caco-2 and T84 intestinal cell lines
638 respectively at an MOI of 1 to 10. **B, D.** Invasion assays were performed with Caco-2 and T84
639 intestinal cell lines respectively at an MOI of 1 to 10. The percentage of adhered and invasive
640 bacteria were calculated based on the initial inoculum and expressed relative to the value for the
641 WT strain. All data are from independent experiments (n=9, each with 3 technical replicates).
642 The error bars indicate the 95% confidence intervals of the means of the wells. Data were
643 analyzed using the Mann-Whitney U test (****, $p < 0.0001$).

644

645

646

647

648

649

650

651

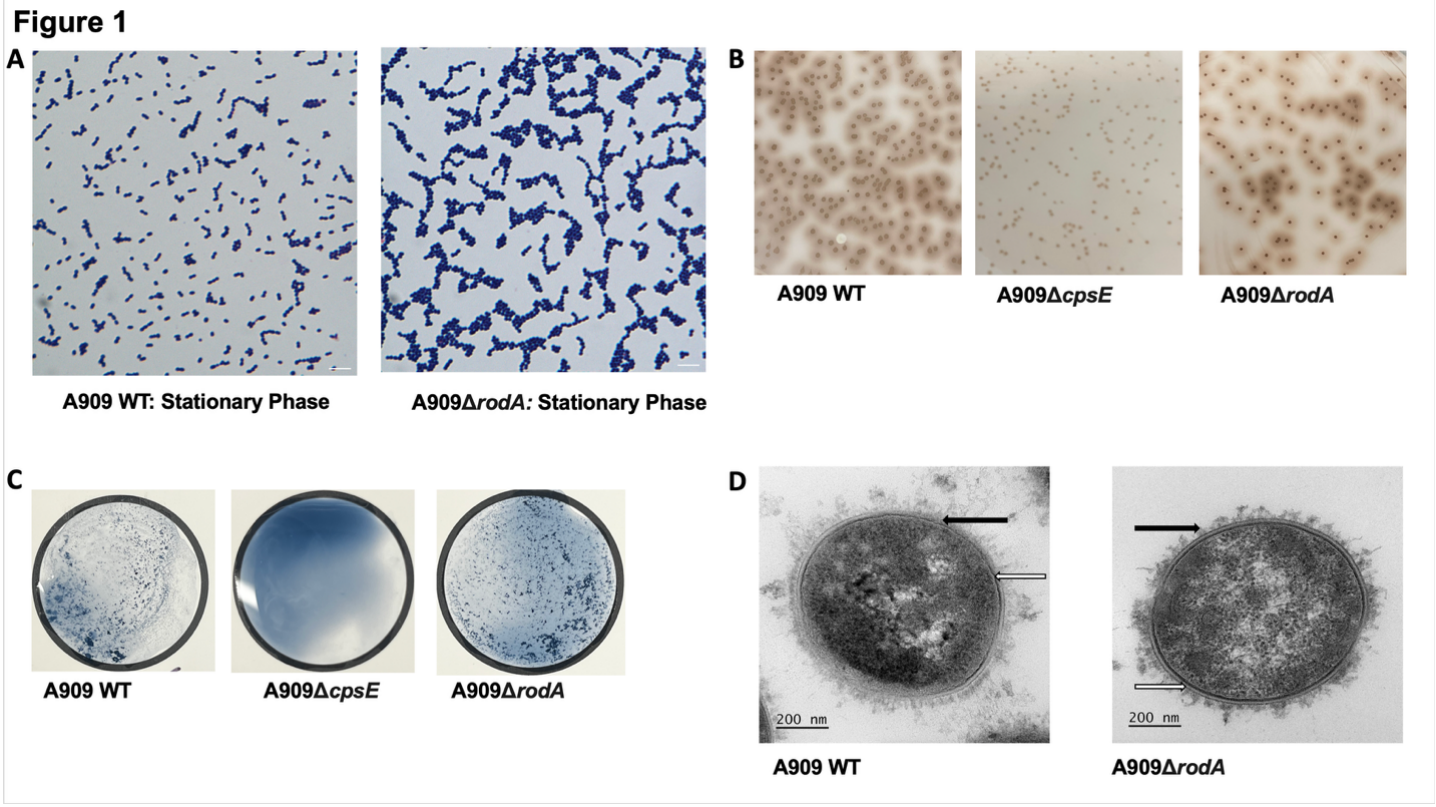

652

653

654

655

656

657

658

659

660
661
662

Figure 2

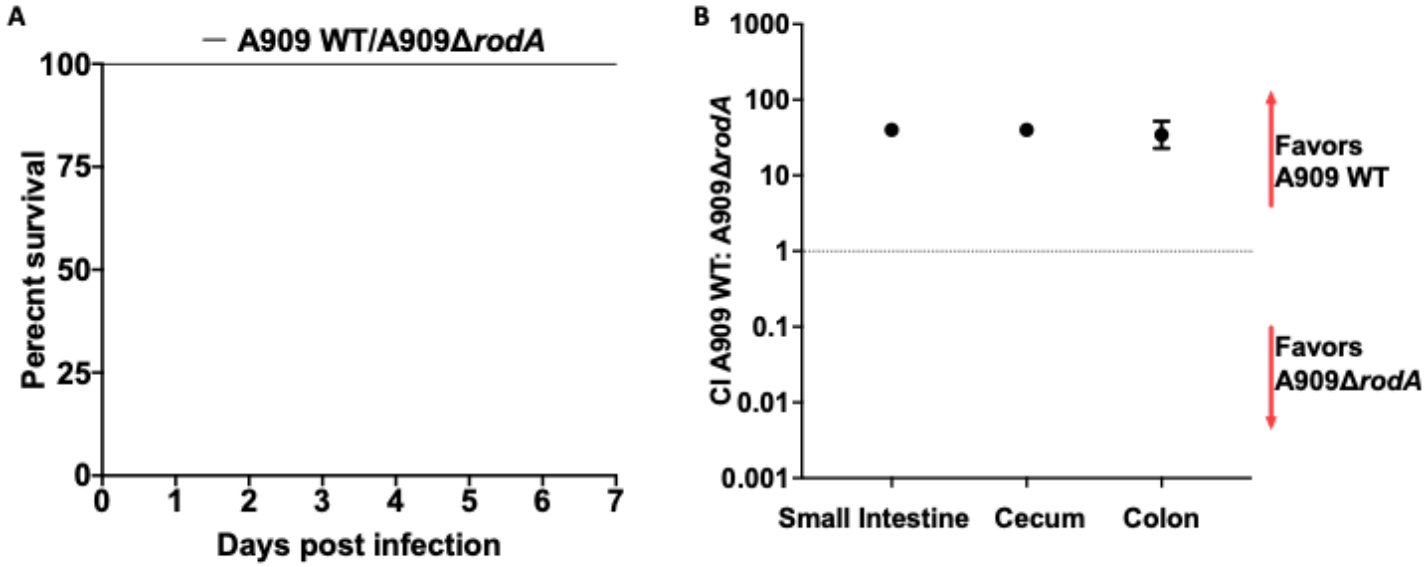

663
664
665
666
667
668
669
670

Figure 3

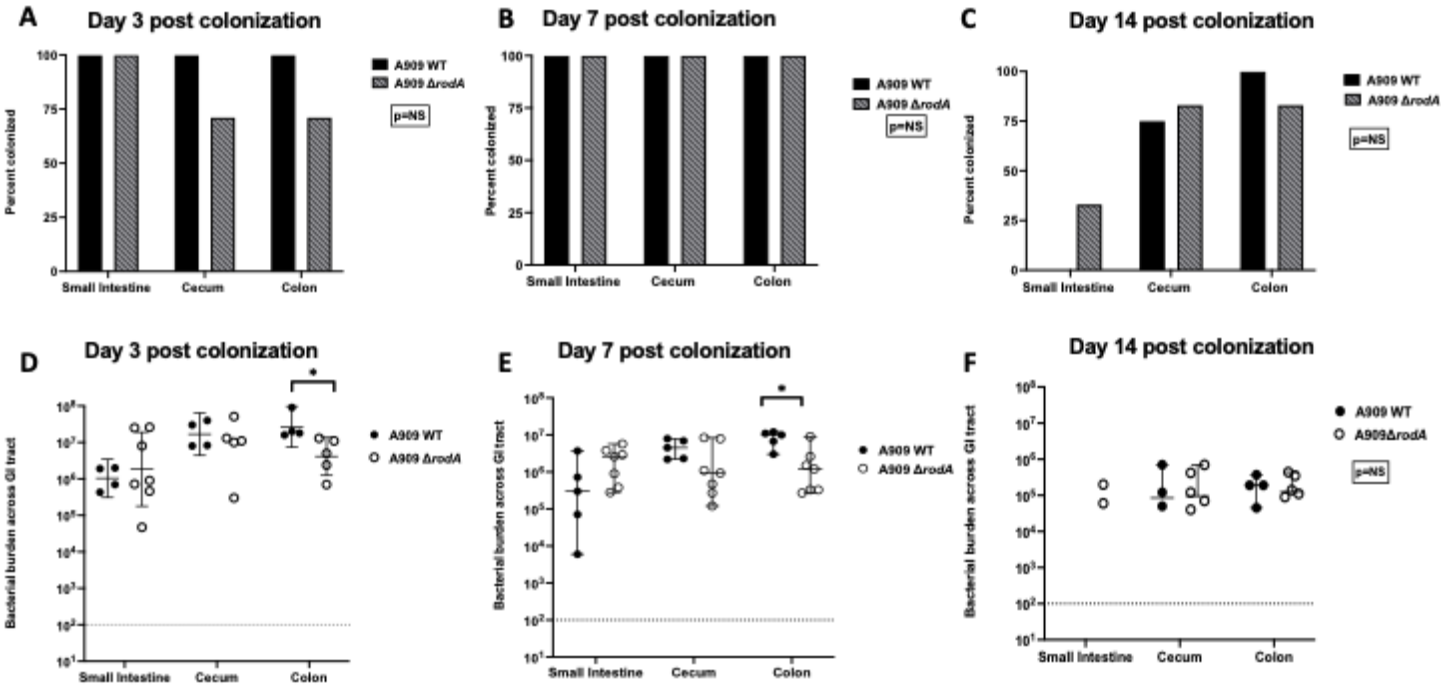
A
Day 3 post colonization
Percent colonized
A909 WT
A909 ΔrodA
p=NS
Small Intestine
Cecum
Colon
B
Day 7 post colonization
C
Day 14 post colonization
D
Day 3 post colonization
Bacterial burden across GI tract
E
Day 7 post colonization
F
Day 14 post colonization

Figure 4

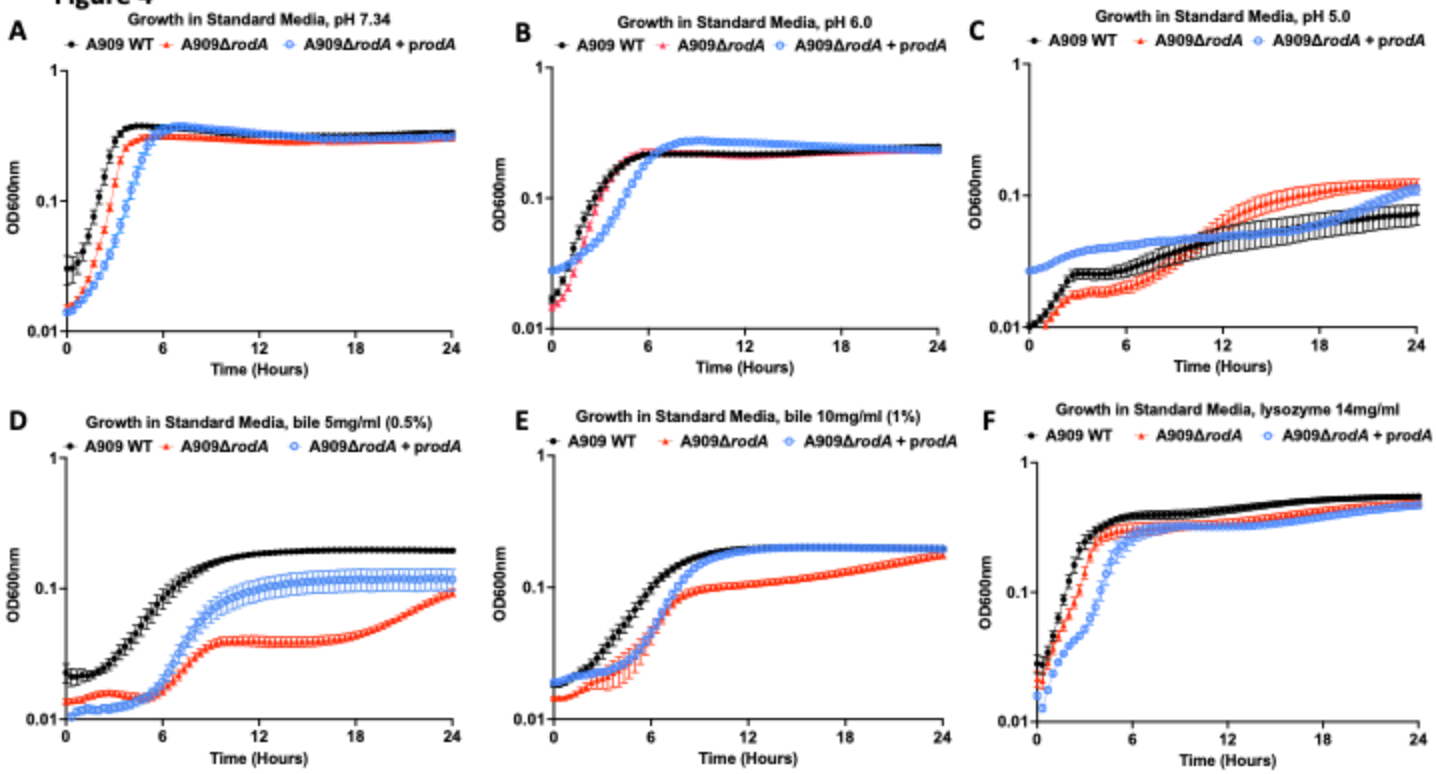
A
Growth in Standard Media, pH 7.34
A909 WT
A909ΔrodA
A909ΔrodA + prodA
OD600nm
Time (Hours)
B
Growth in Standard Media, pH 6.0
C
Growth in Standard Media, pH 5.0
D
Growth in Standard Media, bile 5mg/ml (0.5%)
E
Growth in Standard Media, bile 10mg/ml (1%)
F
Growth in Standard Media, lysozyme 14mg/ml

Figure 5

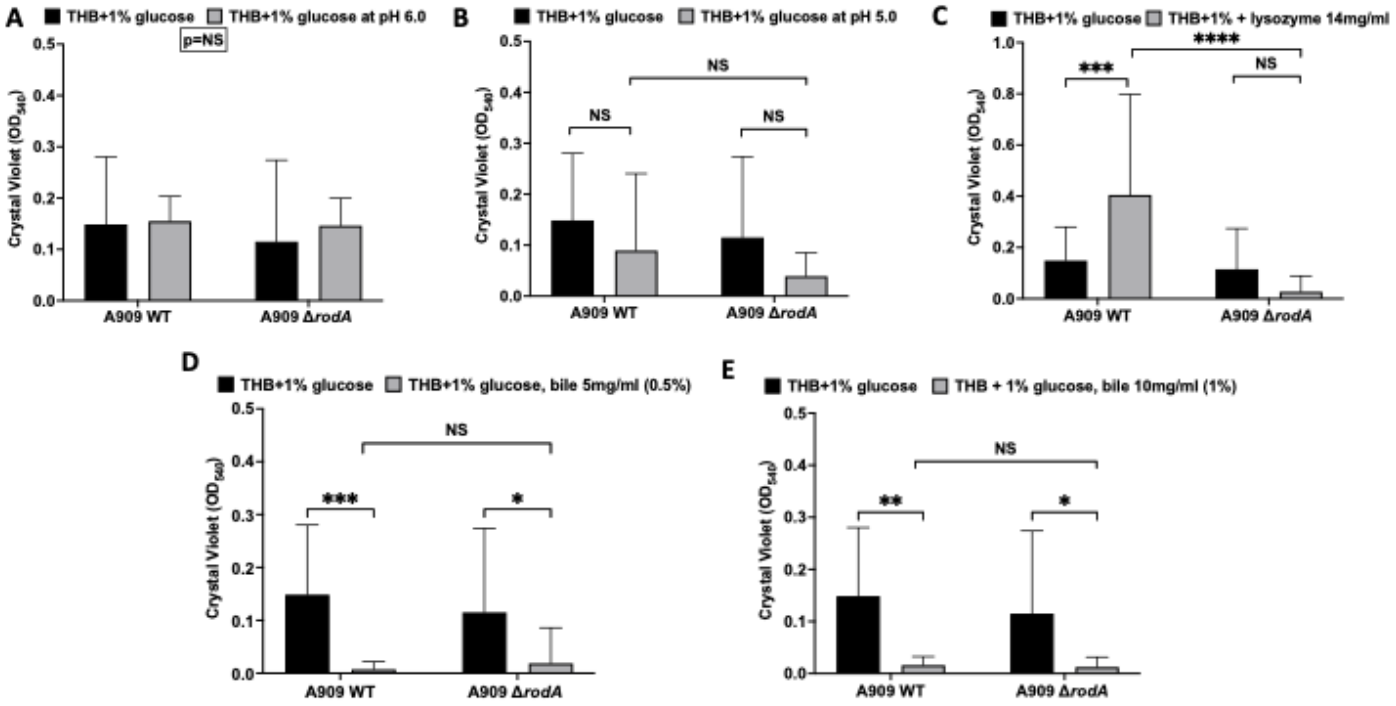
A
THB+1% glucose
THB+1% glucose at pH 6.0
p=NS
Crystal Violet (OD540)
A909 WT
A909 ΔrodA
B
THB+1% glucose
THB+1% glucose at pH 5.0
NS
NS
NS
C
THB+1% glucose
THB+1% + lysozyme 14mg/ml
****
***
NS
D
THB+1% glucose
THB+1% glucose, bile 5mg/ml (0.5%)
NS
***
*
E
THB+1% glucose
THB + 1% glucose, bile 10mg/ml (1%)
NS
**
*

Figure 6

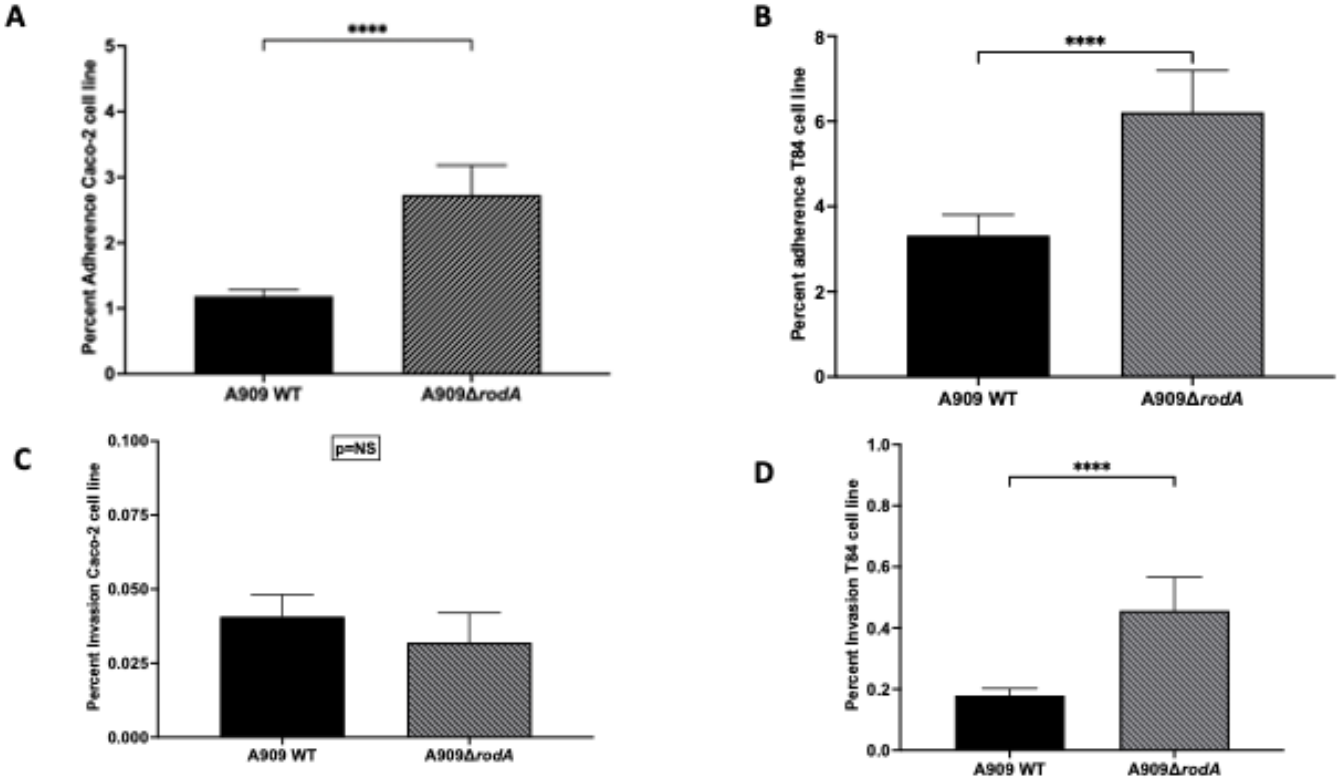

729
730
731